



Published in final edited form as:

Biomaterials. 2011 October ; 32(30): 7479–7490. doi:10.1016/j.biomaterials.2011.06.034.

SAM-based Cell Transfer to Photopatterned Hydrogels for Microengineering Vascular-Like Structures

Nasser Sadr^{1,2,3,4}, Mojun Zhu⁵, Tatsuya Osaki⁶, Takahiro Kakegawa⁶, Yunzhi Yang⁷, Matteo Moretti⁸, Junji Fukuda^{1,6,*}, and Ali Khademhosseini^{1,2,3,*}

¹Center for Biomedical Engineering, Department of Medicine, Brigham and Women's Hospital, Harvard Medical School, Cambridge, MA, 02139, USA

²Harvard-MIT Division of Health Sciences and Technology, Massachusetts Institute of Technology, Cambridge, MA, 02139, USA

³Wyss Institute for Biologically Inspired Engineering, Harvard University, Cambridge, MA, 02139, USA

⁴Bioengineering Department, Politecnico di Milano, Piazza Leonardo da Vinci 32, 20131 Milan, Italy

⁵Department of Biology, Mount Holyoke College, South Hadley, MA 01075, USA

⁶Graduate School of Pure and Applied Sciences, University of Tsukuba, 1-1-1 Tennodai, Tsukuba, Ibaraki 305-8573, Japan

⁷Department of Restorative Dentistry and Biomaterials, University of Texas Health Science Center at Houston, TX 77030, USA

⁸Cell and tissue engineering laboratory, IRCCS Istituto Ortopedico Galeazzi, Via Galeazzi 4, 20161 Milan, Italy

Abstract

A major challenge in tissue engineering is to reproduce the native 3D microvascular architecture fundamental for *in vivo* functions. Current approaches still lack a network of perfusable vessels with native 3D structural organization. Here we present a new method combining self-assembled monolayer (SAM)-based cell transfer and gelatin methacrylate hydrogel photopatterning techniques for microengineering vascular structures. Human umbilical vein cell (HUVEC) transfer from oligopeptide SAM-coated surfaces to the hydrogel revealed two SAM desorption mechanisms: photoinduced and electrochemically triggered. The former, occurs concomitantly to hydrogel photocrosslinking, and resulted in efficient (>97%) monolayer transfer. The latter, prompted by additional potential application, preserved cell morphology and maintained high transfer efficiency of VE-cadherin positive monolayers over longer culture periods. This approach

© 2011 Elsevier Ltd. All rights reserved.

*Correspondence should be addressed to: Junji Fukuda (fukuda@ims.tsukuba.ac.jp), 1-1-1 Tennodai, Tsukuba, Ibaraki 305-8573, Japan, Ali Khademhosseini (alik@rics.bwh.harvard.edu), 65 Landsdowne Street, Cambridge, MA 02139, USA.

Author Contribution

NS, MM, JF and AK designed the study with the contribution of YY; NS and MZ performed the experiments; TO and TK gold coated glass substrates and fabricated culture chambers, NS and MZ analyzed the data; NS wrote the paper; MZ, YY, MM, JF and AK revised the paper. All the authors discussed the results and commented on the paper.

Publisher's Disclaimer: This is a PDF file of an unedited manuscript that has been accepted for publication. As a service to our customers we are providing this early version of the manuscript. The manuscript will undergo copyediting, typesetting, and review of the resulting proof before it is published in its final citable form. Please note that during the production process errors may be discovered which could affect the content, and all legal disclaimers that apply to the journal pertain.

was also applied to transfer HUVECs to 3D geometrically defined vascular-like structures in hydrogels, which were then maintained in perfusion culture for 15 days. As a step toward more complex constructs, a cell-laden hydrogel layer was photopatterned around the endothelialized channel to mimic the vascular smooth muscle structure of distal arterioles. This study shows that the coupling of the SAM-based cell transfer and hydrogel photocrosslinking could potentially open up new avenues in engineering more complex, vascularized tissue constructs for regenerative medicine and tissue engineering applications.

Keywords

Photocrosslinkable hydrogel; zwitterionic oligopeptide; electrochemical cell detachment; gelatin methacrylate; vascular microengineering; endothelial monolayer

1. Introduction

A major challenge in engineering functional tissues *in vitro* is to mimic the underlying *in vivo* 3D microarchitecture. Vasculature represents an outstanding example of complex spatially organized cellular/ECM structures, and their successful generation *in vitro* is known to be crucial for a range of applications such as regenerative medicine and drug discovery [1].

Self-organization of endothelial cells on 2D or within 3D biological gels is by far the most common approach to promote vascularization and angiogenic processes in engineered tissues [2]. However, the extensive culture time needed to allow cell migration and organization, the lack of control on 3D tubular organization, along with the limitations in attaining perfusable vessels *in vitro*, have so far hindered a successful transfer of this approach to tissue engineering applications.

These constraints have prompted the exploration of alternative approaches, often relying on microengineering techniques to fabricate vascularized tissue constructs. For instance the modular assembly of micrometric organoids covered with endothelial cells has been shown to enable blood perfusion [3]. More recently, engineered perfusable microvessels were generated by seeding endothelial cells in microfluidic collagen gels and then successfully adopted to investigate the role of cyclic AMP in vascular barrier regulation [4]. However, seeding-based approaches can often be characterized by complex procedures or rely on several days of culture to form an endothelial monolayer [5]. Applying bioprinting principles, Norotte and colleagues fabricated hollow vascular structures by substituting cell seeding with the precise deposition of micron-sized cellular cylinders around an agarose molding template [6]. These approaches, which rely on complex and expensive instrumentation, so far have not been applied to the generation of vascular constructs lined with endothelial cell monolayer. Nonetheless, an *in vivo*-like endothelial monolayer would be critical to recapitulate native blood vessel functions such as the regulation of diffusion and extravasation processes.

As an alternative approach, we have recently demonstrated the generation of vascular-like structures by transfer of endothelial monolayers from gold rods to the internal surfaces of micrometric collagen channels [7]. This microengineering approach uses culture substrates modified with self-assembled monolayers (SAMs) of alkanethiol or oligopeptides that mediate cell detachment once electrochemically desorbed [8, 9]. Cells can then be deposited on a receiving substrate with an approach similar to thermoresponsive polymer-based cell sheet engineering [10].

Here we studied the integration of zwitterionic oligopeptide SAM-based cell deposition with the photoinduced hydrogel crosslinking process. Hydrogels, indeed, provide a flexible microfabrication platform that can be applied to the generation of geometrically defined three dimensional (3D) constructs [11, 12] and microfluidic channels [13]. In addition, due to the rapid hydrogel crosslinking, photoactivated approaches offer the advantage of minimized processing time. This is a critical parameter while engineering thick tissues with a high number of metabolically active cells that would benefit from the immediate onset of perfusion culture. More specifically, here we have adopted a previously developed gelatin methacrylate hydrogel, that has been shown to be cell adhesive and support proliferation of cells seeded on the surface and of those encapsulated within the gel [14]. We first investigated mechanisms responsible for the SAM-based cell detachment in transfer of single cells and monolayers from gold to hydrogel. The association of the SAM-based cell deposition and hydrogel photocrosslinking was further applied to the generation of micrometric single and double vascular structures.

2. Materials and methods

2.1 Materials and reagents

Glass slides (24 mm × 24 mm; No. 4) from Matsunami Glass (Japan), glass rods (diameter, 600 μm; length, 3.2 cm) from Hirschmann Laborgeräte (Germany), and synthetic oligopeptide, CGGGKEKEKEKGRGDSP, from Sigma-Aldrich (Japan) were used to fabricate culture substrates. Endothelial basal medium-2 (EBM-2, CC-3156) and SingleQuots growth supplement (CC-3162) from Lonza (Switzerland) were used for cell culture. Gelatin (Type A, 300 bloom, from porcine skin) and methacrylic anhydride were purchased from Sigma Aldrich (USA) for methacrylated gelatin (GelMA) synthesis. Irgacure 2959 photoinitiator (2-hydroxy-1-(4-(hydroxyethoxy) phenyl)-2-methyl-1-propanone, CIBA Chemicals) was initiated by a ultraviolet (UV) light source (Omniscure S2000) from EXFO Photonic Solutions Inc. (Canada) for polymer photocrosslinking. All other chemicals were purchased from Sigma-Aldrich (USA) unless otherwise indicated.

2.2 Methacrylated gelatin synthesis and prepolymer solution preparation

GelMA was synthesized as previously described [14–16]. Briefly, type A porcine skin gelatin was added (10% w/v) to Dulbecco's phosphate buffered saline (PBS; GIBCO, USA), heated at 60 °C, and stirred for 1 h. Methacrylic anhydride was added (7.5% v/v) at a rate of 0.5 ml/min to the gelatin solution at 50 °C while stirring and allowed to react for 2 h. Samples were then dialyzed in 12–14 kDa cutoff dialysis tubing in distilled water at 40 °C for 1 week before being filtered (0.2 μm). Finally, the solution was frozen overnight (−80 °C), lyophilized for 1 week, and stored at −80 °C until further use.

A prewarmed (60 °C) 0.05% (w/v) photoinitiator (PI) solution in PBS (with Ca Mg) was mixed with GelMA macromers (5% w/v) until fully dissolved and was used when cooled to room temperature. Fresh prepolymer solution was prepared for each experiment.

2.3 Peptide design and gold surface modification

Gold substrates were prepared by sputter coating Cr (1 nm layer) and Au (40 nm layer) on glass slides and glass rods, which were pre-cleaned with ammonia/peroxide mix (NH₄OH/H₂O₂/H₂O, 1/1/4) [7, 9]. The oligopeptide (CGGGKEKEKEKGRGDSP) consists of three main functional domains, designed to generate SAMs on gold that prevent non-specific protein adsorption while exclusively mediate cell adhesion. On one end of the oligopeptide, cysteine has a thiol group that adsorbs to gold surface via a gold–thiolate (S–Au) bond (Fig. 1A). The central domain, composed of charged glutamic acid (E) and lysine (K) residues, promotes electrostatic packing of adjacent peptides, which enhances the non-fouling

properties [17] of SAM. On the other end, the RGD motif mediates cell adhesion by interacting with integrins expressed on cell surface. Peptide adsorption does not require any organic chemistry and was obtained by incubating gold substrates in 5 μM aqueous oligopeptide solution at 4 $^{\circ}\text{C}$ for 16 h. Before cell seeding, the substrates were rinsed twice with pure water, once in 70% ethanol, and twice in PBS.

2.4 Cell culture

Immortalized human umbilical vein endothelial cells (HUVECs; a generous gift from Dr. J. Folkman, Children's Hospital, Boston) constitutively expressing green fluorescent protein (GFP) were cultured in EBM-2 supplemented with SingleQuots growth supplement. NIH 3T3 fibroblasts were cultured in Dulbecco's modified Eagle medium (GIBCO, USA) supplemented with 10% fetal bovine serum (Gibco, USA) and 1% Penicillin/Streptomycin (Gibco, USA). All cells were cultured in standard cell culture incubators (5% CO_2 , 37 $^{\circ}\text{C}$). Culture medium was changed every 48 h, and cells were passaged when 60–70% confluence was reached.

2.5 Self-assembled monolayer stability

To evaluate SAM stability in a solution containing PI when exposed to UV (PI&UV), mass adsorption/desorption experiments and surface chemical characterization were performed. A Quartz Crystal Microbalance (QCM; Q-sense E4, Biolin Scientific/Q-Sense, Sweden) equipped with open measuring modules and gold coated sensors was used to measure the resonant frequencies of bare gold in double distilled water (ddH_2O). After incubation in the oligopeptide solution (5 μM) at 24 $^{\circ}\text{C}$ for 3 h, the sensors were rinsed with ddH_2O before measuring the resonant frequencies. Sensors were then exposed to PI&UV (0.05% w/v; 50 s, 6.5 mW/cm^2) and rinsed in ddH_2O before the final measurement.

Modified gold substrates were analyzed with X-ray photoelectron spectroscopy after PI&UV exposure. They were compared to those that were simply immersed in PBS. Samples were rinsed with ddH_2O and dried under N_2 before being analyzed by the spectrometer. X-ray photoelectron spectra were recorded using a Kratos AXIS Ultra spectrometer (Kratos Analytical Ltd, UK) with charge neutralizer. Oxygen (O1s), carbon (C1s), nitrogen (N1s), and gold (Au4f) spectra were obtained with a monochromatic Al K α X-ray source (1486.6 eV) and pass energy of 20.0 eV. All spectra were calibrated with reference to Au4f at a binding energy of 83.65 eV. Spectra were obtained with similar settings (number of sweeps, integration times, etc.) for each sample and normalized to the Au 4f peak.

To investigate cell adhesion on gold substrates in the presence of PI&UV, HUVECs were seeded at a density of 7.5×10^4 cells/ml (2-ml for each well, 15.6×10^3 cells/ cm^2) on gold coated glass slides modified with the oligopeptide. After 16-h incubation in a 5% CO_2 incubator at 37 $^{\circ}\text{C}$, non-adherent cells were removed by aspirating the medium and rinsing in PBS (with Ca Mg). The samples were then immersed in PI solution (0.05% w/v) and exposed to UV for 50 s (6.5 mW/cm^2). Following irradiation, the samples were rinsed with PBS (with Ca Mg). Phase-contrast images of the gold surface were taken immediately before and after the procedure to investigate cell detachment and morphology. Non-modified gold substrates (with and without PI and UV) and modified substrates (without PI and UV, immersed in PBS) were adopted as controls.

2.6 Two dimensional cell transfer

Oligopeptide modified gold substrates were seeded with HUVECs (15.6×10^3 cells/ cm^2) and incubated for 16 h. After rinsing samples in PBS (with Ca Mg), the GelMA prepolymer solution (800 μl) was poured onto the surface (confined by a polydimethylsiloxane, PDMS,

mold 18 × 18 mm) and UV photocrosslinked for 50 s (6.5 mW/cm²). Samples were then immersed in PBS (with Ca Mg) either with or without −1.0 V potential application (potentiostat, model 1100, Fuso Mfg. Co., Japan) for 2 min (Fig. 1B), followed by hydrogel layer removal from the substrate. Samples without oligopeptide modification were adopted as controls.

Phase-contrast images at five different fields on the gold surface (immediately before and after cell transfer) and the hydrogel surface (immediately after each transfer) were acquired (MetaMorph[®], Molecular Devices Inc., USA) by means of an inverted microscope (Axio Observer Z1, Carl Zeiss MicroImaging Inc., USA) equipped with a Cool Snap HQ² camera (Photometrics, USA) and a 10X lens (EC Plan-Neofluar 10X/0.3, Carl Zeiss MicroImaging Inc., USA). The number of cells per field of view was determined using the NIH ImageJ software. Transfer efficiency was expressed as a percentage of mean cell density on the hydrogel after cell transfer over the mean cell density on the corresponding gold surface before cell transfer.

Images of fluorescent GFP cells on gold (before cell transfer) and hydrogel (after cell transfer) were acquired (same settings) and employed to quantify individual cell area using ImageJ. The total number of cells evaluated was 691 for non-modified gold and 549 for gold coated with the peptide. On hydrogels, the total number of cells evaluated to calculate the cell area was 36 for hydrogel transferred from non-modified gold, while for modified gold it was respectively 707 for hydrogel transferred without and 1121 for those with potential.

Cell viability 2 h after transfer to the hydrogel was investigated with ethidium homodimer-1 (EthD-1) staining (LIVE/DEAD[®], Molecular Probes[®], USA). Fluorescent images were acquired with both GFP and DS-RED filter cubes. Merged images were used to quantify cell viability as the percentage of EthD-1 negative cells over total number of cells.

Cell proliferation and long term viability of samples transferred with and without potential, from oligopeptide modified substrates, were evaluated for up to 72 h after cell transfer. Phase images were acquired at 0, 12, 24, 48 and 72 h. The number of cells per surface area was calculated at each time point and the percentage of spreading population was computed at 12 h. After 72 h, samples were stained with EthD-1 and the cell viability was calculated.

Experiments were run in triplicate for each condition.

2.7 Cell monolayer transfer

To evaluate the transfer efficiency for cell monolayer rather than single cells, gold coated glass slides modified with the oligopeptide were seeded either as described previously and cultured for 72 h, or at a high density (5×10^5 cells/ml, 2-ml for each well) and cultured for 16 h. After rinsing in PBS (with Ca Mg), the confluent cell layers were transferred either with or without potential application. Phase images were acquired before and after cell transfer and used to quantify cell transfer efficiency.

To evaluate the effect of cell transfer process on cell-cell junctions, cellular monolayers on gold substrates and on hydrogels (incubated 2 h in media after transfer), were fixed in paraformaldehyde (4%, 7 minutes) and immunostained with primary antibodies for VE-Cadherin (VE-Cad rabbit anti-human, Cayman Chemical Company, USA) or Connexin 43 (Cx43; rabbit anti-human, Abcam Inc, USA) and fluorophore conjugated secondary antibody (Cy5 goat anti-rabbit, Abcam Inc, USA), and counterstained with DAPI. All the experiments described above were run in triplicate for each experimental group. Images were taken with a confocal microscope (Leica SP5 X MP, Leica Microsystems, Wetzlar, Germany).

2.8 Microvascular structure generation

HUVECs were seeded on gold rods, modified with the oligopeptide as described for the gold slides, at a density of 1.5×10^5 cells/ml (6 ml for each petri dish) in ultra-low attachment 60 mm dishes (Corning, USA). The culture medium was changed after 24 h to remove excess cells and then every 48 h until confluence (3 to 4 days).

The chamber for perfusion culture ($2.5 \times 10 \times 10$ mm inner dimensions) was fabricated with poly(methyl methacrylate) (PMMA) plates using computer-aided laser machining (Laser PRO C180; GCC, Taiwan). To generate microvascular structures, gold rods with confluent cell layers were placed in the chamber, 250 μ l of prepolymer solution dispensed in the chamber, and UV photocrosslinked for 50 s (6.5 mW/cm^2). Following hydrogel formation, the rods were extracted after potential application (-1.0 V , 5 min). Chambers were then connected to a microsyringe pump and perfused with medium at $2 \mu\text{L/min}$ (Fig. 1C).

Phase-contrast and fluorescent images of the construct were taken with an inverted microscope. The entire construct was visualized 12 h after cell transfer with a confocal microscope. After 15 days in culture, cell-laden hydrogels were fixed in paraformaldehyde (4%, 20 minutes) stained with DAPI and analyzed with an inverted microscope.

To generate complex 3D vascular structures double-layer cell microvascular structures were fabricated (Fig. 1D). In particular, NIH 3T3-fibroblasts that were stained with PKH26 red fluorescent membrane labeling (Sigma-Aldrich) were resuspended in GelMA solution (4×10^7 cells/ml) and then cooled to $18 \text{ }^\circ\text{C}$ to induce partial gelation. Modified gold rods with HUVEC monolayer were dipped in prepolymer solution, placed in the chamber, and photocrosslinked for 40 s (6.5 mW/cm^2). The chamber was then filled with prepolymer solution and UV photocrosslinked for 50 s. Fluorescent images of the construct were taken with an inverted microscope after the first photocrosslinking step. Cross-sectional images of the finished construct were taken with a confocal microscope and a 10X lens.

2.9 Statistics

Statistical significance was determined for replicates of 3 by an independent Student t-test for two groups of data or analysis of variance (ANOVA) followed by Bonferroni's post-hoc test for multiple comparisons using SigmaStat 3.0 (Systat Software, USA). Differences were considered significant for $p < 0.05$.

3. Results and discussion

3.1 Effect of photoinitiator and UV on self-assembled monolayer

Hydrogel photocrosslinking relies on UV induced radical formation of photoinitiator molecules [18], that initiates the formation of a polymer network [19, 20]. However, besides electrochemical desorption, thiolate SAM removal from metal substrates can occur when the substrate is exposed to UV irradiation [21, 22], a phenomenon that has been exploited in alkanethiol UV photopatterning [23]. In the attempt to combine the techniques of hydrogel photocrosslinking and SAM electrochemical cell patterning, it is therefore essential to characterize the possible effects of UV irradiation in the presence of PI (PI&UV) on SAM.

To assess the effect of PI&UV on SAM, oligopeptide modified substrates were exposed to UV in PI solution (in the absence of GelMA prepolymer) at the same conditions adopted for hydrogel photopolymerization. SAM stability was investigated with QCM mass adsorption/desorption and XPS surface chemistry analyses. QCM analysis showed that the resonant frequency of bare gold sensors (Fig. 2A.I) decreased after being immersed in the oligopeptide solution (Fig. 2AII–III) as a result of SAM adsorption on the surface [7]. When

the oligopeptide modified substrate was exposed to PI&UV, the resonant frequency increased, and the initial shift was partially reduced (28.0 ± 5.1 %) (Fig. 2A.IV), indicating a loss of the adsorbed mass from the gold surface. Also XPS analysis revealed a change in the surface chemistry of SAM modified gold substrates exposed to PI&UV. Spectrum peaks of peptide constituents such as carbon, oxygen, and nitrogen decreased compared to the controls rinsed in PBS (Fig. 2B), with a calculated loss of surface mass concentration of 22.7% (carbon), 13.8% (oxygen), and 3.2% (nitrogen). These observations suggest that UV irradiation in the presence of PI can affect oligopeptide SAM coating on gold substrates, resulting in a partial desorption of the adsorbed peptides. Previous studies on UV effects on alkanethiol molecule have identified photo-oxidation of the S-Au bond as the major reason for SAM desorption, but the exact mechanism is still not clear [24, 25]. Other bond scissions (such as C-S bond) have also been indicated to contribute to the process [26]. However, since our experimental conditions differ from previously reported studies, SAM desorption might have occurred via alternative mechanisms.

To evaluate the influence of photoinitiated SAM desorption on cell adhesion, HUVECs were seeded at a low density (15.6×10^3 cells/cm²) on gold surfaces. Cells readily adhered (sparse adherent cell population with negligible cell-cell contact) and acquired a spread morphology (Fig. 2D). After 16 h, substrates were irradiated with UV in a PI solution without GelMA prepolymer (PI concentration and UV exposure identical to those used for GelMA photopolymerization). Analysis of phase contrast images taken before and after PI&UV exposure show a significantly decreased cell population (71.9 ± 3.4 %) on SAM modified gold substrates characterized by a rounded morphology (Fig. 2C,E). When submerged in PBS in the absence of PI&UV, cells remained adherent and maintained a spread morphology (Fig. 2C,F) supporting the role of PI&UV in the detachment process. Finally, cells cultured on non-modified substrates did not detach or change morphology when exposed to PI&UV (Fig. 2G). These results indicate that cell detachment and morphology rearrangement originate from the interactions among peptide, PI, and UV, rather than from peptide-independent mechanisms such as a cytotoxic effect of PI and UV.

Together these findings confirm that PI&UV, crucial to hydrogel photopolymerization, are involved in the partial desorption of SAM. Our results suggest also that this process leads to the loss of oligopeptide-mediated cell adhesion sites, resulting in a more rounded cell morphology and partial cell detachment. This phenomenon could constitute a mechanism additional to electrochemical SAM desorption, contributing to cell transfer to the hydrogel.

3.2 Cell transfer

To probe cell transfer from modified and non-modified gold substrates to GelMA hydrogels with and without electrochemical SAM desorption, HUVECs were seeded on both modified and non-modified gold surfaces for 16 h. Cells adhered to the surface and spread in a similar fashion (Fig. 3A–C) under both conditions. After photocrosslinking GelMA solution on HUVECs, an electrical potential (-1.0 V, 2 min) was applied to non-modified ($\text{Pep}^- \text{El}^+$) and modified ($\text{Pep}^+ \text{El}^+$) samples before removing the hydrogel. A third group was prepared with modified samples without electrical potential application ($\text{Pep}^+ \text{El}^-$). Images of the gold surfaces after GelMA removal (Fig. 3D–F) show that most of the cells still adhered to the non-modified gold surface (Fig. 3D), but only a negligible number of cells remained on the modified gold surfaces regardless of the potential application (Fig. 3E,F). Images of the hydrogel after transfer (Fig. 3G–I) show that only 20% of the cells on the non-modified gold surface were transferred to the hydrogel (Fig. 3J). More than 50% of these cells were stained by EthD-1 (Fig. 3K) 2 h after transfer. Both the transfer efficiency and the viability were significantly higher for the surfaces modified with the SAM. Indeed, regardless of whether the potential was applied, almost 100% of the cells were transferred to the GelMA constructs (Fig. 3J) and more than 90% of the cells were viable after 2 h. Samples without

electrical potential application presented slightly lower but not statistically different viability (Fig. 3K). These results underline the importance of the oligopeptide modification process for efficient cell transfer.

To explore the effect of oligopeptide electrochemical cleavage on cell morphology, fluorescent images of the cells seeded on the gold surfaces were analyzed to quantify the mean cell area and its distribution (Fig. 4A,B). The few cells transferred from substrates without oligopeptide modification presented mostly a rounded morphology (Fig. 3G) and a mean area significantly lower than those from the modified substrates (Fig. 4A). For the modified substrates, the electrochemical cleavage of the SAM resulted in a significantly higher mean cell area compared to cells transferred without potential, and an overall cell area distribution closely resembling the one on gold substrates (Fig. 4B) before cell transfer. In addition, the cells transferred with potential application presented a statistically higher percentage of spread cells after 12-h culture (Fig. 4C–E), but no significant difference was observed in terms of proliferation and viability at 72-h culture. Indeed, regardless of electrochemical oligopeptide desorption, the cells proliferated on the hydrogel for 3 days, displaying viability close to 100% (Fig. 4C,F) after 72 h.

Cell transfer is achieved when the cells detach from a substrate and adhere to a new substrate. Previous studies on electrochemically desorbed SAM indicate that cell detachment occurs in two steps: externally triggered cleavage of cell-substrate adhesion sites, followed by an active metabolic driven rearrangement of the cytoskeleton [27]. A similar process has been proposed for thermoresponsive substrates [28], while final cell removal from the substrate has been shown to be dependent on external forces such as those generated by fluid flow or cell-cell interactions [29, 30]. In fact, cell detachment from a substrate and transfer to a new one depends on the balance of interaction forces between cells and each substrate. Recently, Weder *et al.* have quantitatively demonstrated that triggered cell detachment and consequent decreased cell-surface adhesion are crucial to highly efficient cell transfer to a new substrate [31].

In our system, cell transfer occurs when cell-hydrogel interaction forces are greater than cell-gold adhesion forces. When cells adhere to the substrate through non-specifically adsorbed proteins ($\text{Pep}^- \text{EI}^+$), the balance favors cell-gold interactions. Few cells are transferred, and a considerable fraction of the transferred cells presents a compromised membrane, most likely due to mechanical stress as cells are peeled off from the substrate [32]. As the electrical potential is applied on the modified substrate, the gold-thiol bond is reductively cleaved, dramatically reducing cell adhesion, therefore promoting a highly efficient transfer of the cells to the hydrogel with negligible effect on cell viability. Surprisingly, our results pointed out that even in the absence of electrochemical thiol-gold cleavage ($\text{Pep}^+ \text{EI}^-$) the force balance favors cell transfer, with efficiency and viability similar to those obtained with potential application. This finding appears to be coherent with our observations about the UV mediated SAM desorption in PI solution and the consequent partial cell detachment.

Cell transferred to the hydrogel displayed a spread morphology, suggesting that the rapid onset of cell-hydrogel interaction points provides sufficient adhesion sites for maintaining cell area during the transfer. The different cell area after transfer with or without potential may be caused by distinctive residual cell-gold adhesion forces rather than a difference in cell-hydrogel adhesion. Indeed, although electrochemical oligopeptide cleavage was shown to induce almost complete cell detachment [7], only 30% of cells came off with photoinduced SAM desorption (Fig. 2C). The remaining population retained a number of adhesion sites with the gold that could act as traction points during the peeling process, contributing to cell deformation and eventually loss of cell spreading [33, 34]. The dismissal

of electrochemical oligopeptide desorption also led to a slightly lower spread population at 12-h culture but did not affect proliferation and viability over 3 days (Fig. 4C,F).

Overall, these results suggest that the electrochemical SAM desorption step influences the degree of dissociation of cell-gold adhesion sites, which affects the mechanics of cell transfer and therefore the initial cell morphology and spreading. Nevertheless, regardless of potential application, cell transfer from oligopeptide-SAM coated gold substrates to hydrogel is highly efficient and preserves both cell viability and proliferation ability.

3.3 Cell monolayer transfer

HUVEC monolayer transfer from oligopeptide modified substrates to hydrogel was investigated by seeding the cells at a low density (15.6×10^3 cells/cm²) and culturing them for 72 h (LD-72h), or by seeding at a high density (10.4×10^4 cells/cm²) and culturing for 16 h (HD-16h). In both conditions, confluent cell monolayers were obtained by the end of the culture period with similar cell number ($10.26 \pm 0.60 \times 10^4$ cells/cm²). After hydrogel photocrosslinking, samples were transferred either with (Pep⁺ EI⁺) or without (Pep⁺ EI⁻) electrical potential (-1.0 V, 2 min). The results for the HD-16h samples were similar to those obtained with sparse cells. The entire cell population was transferred to the hydrogel regardless of electrochemical oligopeptide desorption and a continuous cell monolayer covering the hydrogel surface (Fig. 5A,B,E) was obtained. The LD-72h samples displayed lower transfer efficiencies than the HD-16h samples, with relevant differences between Pep⁺ EI⁻ and Pep⁺ EI⁺ (Fig. 5C,D). Without electrochemical SAM desorption, only $32.9 \pm 16.4\%$ of the cells were transferred, whereas a significantly higher efficiency was obtained with electrochemical SAM desorption, successfully transferring $80.9 \pm 6.5\%$ of the cells (Fig. 5E). The fraction of HUVECs remaining on the gold substrate suggests that the effect of culture period on transfer efficiency was most likely due to a shift in the hydrogel-cell/cell-gold force balance towards gold.

Whereas cell-gold adhesion forces increase during the first cell spreading and cytoskeleton rearrangement [35], the onset and maturation of cell-cell interactions at later time points have been correlated with decreased cell-substrate interactions [36]. This process has been shown to eventually sustain the cell transfer [37]. Nonetheless, a longer culture time exposes SAM to a greater chance of contamination by proteins from the medium or secreted by the cells [38]. These proteins would behave as non-cleavable anchoring sites that increase cell-gold residual interaction forces, which eventually hinder cell transfer. The effect of these contaminants is expected to be more dramatic without electrochemical SAM desorption since photoinduced oligopeptide desorption has been shown to be only partial, and therefore have constitutively higher residual adhesion forces.

While investigating endothelial monolayer transfer, it is crucial to evaluate the effect of transfer process on cell-cell junctions, a class of proteins vital to monolayer functions. Among the other junctions, VE-Cad adherens junction and Cx43 gap junction play fundamental roles in regulating vascular stability and selective permeability to molecules and cells [39, 40]. To investigate the effect of cell transfer on cell-cell junctions, all HD-16h and LD-72h samples, with the exception of LD-72h Pep⁺ EI⁻, were fixed and stained for VE-Cad and Cx43 before and 2 h after transfer. On gold substrates, the endothelial monolayer exhibited positive VE-Cad staining at cell-cell boundaries (Fig. 5F), confirming the characteristic onset of endothelial monolayer cell-cell junctions for cells cultured on SAM. On the hydrogel, the monolayer still presented a clear VE-Cad positive staining at the cell-cell edges, suggesting that the adherens junctions were preserved over the transfer process both without and with electrochemical desorption at HD-16h (Fig. 5G,H) and for LD-72h when the potential was applied (Pep⁺ EI⁺, Fig. 5I). On the contrary, Cx43, which on gold was mostly restricted to cell-cell boundaries (Fig. 5J), after transfer displaced from the

periphery to the inner compartment of cells, often in proximity to the cell nuclei (Fig. 5K–M). This rearrangement, which occurred independently from the transfer condition, is typical of connexin internalization. This process was shown to be transiently increased by UV exposure, peaking at 2 h and returning to baseline values after 8 h [41], as part of the gap junction dynamic synthesis-proteolysis [42].

Although previous studies have described successful applications of endothelial cell transfer in tissue engineering [37, 43, 44], their approaches mostly depend on active cell migration, a process that required significantly longer transfer time (up to 24 h) and a meticulous design for cell relative binding affinity to initial and receiving substrates. The introduction of a triggered detachment process enables a controlled transfer of the endothelial cell monolayer from oligopeptide coated gold substrate to photocrosslinkable GelMA within few minutes. High efficiency can be obtained relying either on a photoinduced partial SAM desorption or on its combination with electrochemical oligopeptide cleavage. While the photoinduced mechanism alone eliminates the need for electrical connections and equipment, our results established that the combination of photo- and electrical SAM desorption preserves higher cell transfer efficiency over time. Besides this, both approaches were shown to conserve VE-Cad junctions, critical to cell-cell communication, monolayer maturation, vascular generation and physiological functions. Considering the central role of cell-cell junctions in vascular function, further studies are needed to evaluate the junction rearrangement, focusing specifically on Cx43, a highly dynamic junction, which was currently shown to be disrupted during the cell transfer process.

3.4 Microvascular structure generation

After characterizing the transfer process on 2D substrate, the combination of SAM-based cell transfer and hydrogel photopatterning was investigated in a more complex 3D setting as a platform for rapidly engineering *in vitro* vessels, featuring a readily available hollow structure and controlled geometrical design. Gold sputtered rods, with a diameter of 600 μm , were modified with the oligopeptide, seeded with HUVECs and then cultured in petri dishes (3–4 days) until uniformly covered by a confluent endothelial monolayer (Fig. 6A). Based on the previously described results concerning the effect of culture time on cell transfer, after GelMA photocrosslinking, we applied a -1.0 V potential to achieve optimal HUVECs transfer. Following the removal of the rod, tubular structures completely lined with an endothelial monolayer were obtained, having a length of 10 mm and a diameter of 618 ± 15 μm (Fig. 6B). The geometry of the channels was stable as no deformations or shrinkages were observed following the fabrication process. Mimicking *in vivo* conditions, cultured samples were maintained under perfusion for up to 15 days. Confocal images acquired at 12 h show that HUVECs displayed a spread morphology and covered the inner surface of the channel with no particular signs of cell detachment or wash out (Fig. 6C), thus suggesting sufficient construct oxygenation and the absence of detrimental effects of toxic photopolymerization residues. Representative images of construct sections show a cell monolayer lining on the inner surface of the channel (Fig. 6D), accurately replicating the circular cross-section of the rod and mimicking the arrangement of endothelial cells *in vivo*, while volumetric reconstructions illustrate the hollow tubular cell monolayer (Fig. 6E). Images after 5 days of culture show a compact cell population completely lining the hydrogel surface (Fig. 6F). The constructs maintained a stable geometry over the 15-day culture with no evidence of channel deformation due to hydrogel collapse or cell layer detachment. Indeed, even after 15 days of culture the engineered vascular structure displayed a hollow channel encircled by cells (Fig. 6G). Dissimilarly from our previous experiments with collagen [7] cells did not invade the hydrogel even at the latest time points. Due to the absence of cell-cell contact proliferation inhibition, typical of

immortalized cell line, the HUVECs were rather prone to grow into a multicellular endothelial layer.

To investigate if the proposed hydrogel photopatterning could be adapted to microengineer *in vitro* the complex multilayered geometrical organization of blood vessels, double layer cell constructs were generated by adding a cell laden hydrogel stratum encircling the endothelial monolayer. Adopting a dip-coating approach, namely the immersion/withdrawal of HUVEC confluent gold rods in a 3T3 cell-GelMA prepolymer suspension, cell suspension was conveyed onto the rod surface, obtaining uniform second cell layers that were immediately photocrosslinked (Fig. 6H). The thickness of the deposited layer, in a dip-coating approach, is known to be primarily determined by fluid viscosity, which in our case mainly depends on prepolymer concentration and solution temperature, adjusted in our experiments to obtain a thickness of one to three cells. The double layer constructs were embedded in hydrogel as previously described. After potential application and rod removal, channels with an outer 3T3-cell layer (Fig. 6I) lined with an inner HUVEC monolayer (Fig. 6J) were obtained. The composed image of the two layers shows that the external layer creates a homogeneous cellular frame (one to three cell thick) in close geometrical proximity with the endothelial layer (evidenced also by partial fluorescence overlap) (Fig. 6K). This organization mimics well the structural arrangement of distal arterioles, characterized *in vivo* by an endothelial monolayer encircled by one to two layers of smooth muscle cells.

As previously mentioned, current approaches for generation of vascular structures suffer from several limitations such as the lack of control on 3D tubular organization and the extensive culture time required for the arrangement of endothelial cell monolayer into patent vascular structures [1, 5]. Our results show that the combination of hydrogel photopolymerization and SAM-based cell transfer dramatically shortens the process to generate *in vitro* vascular-like structures lined with endothelial cell monolayers. Moreover, the proposed method provides a precise and stable geometrical outline of vascular structures. This crucial attribute determines fluidodynamic conditions, critical to vascular construct designed for *in vitro* models [45, 46] as well as for *in vivo* applications [47]. Furthermore, the conjunction of rapid polymerization with high geometrical control paves the way to the design of more challenging 3D vascular architectures. As a proof of concept, the photopatterning was extended to the generation of double-layer constructs, demonstrating that the approach could represent a microengineering platform that more closely mimics *in vivo* microvascular organization. Indeed, endothelial cells are in most of the cases just the inner layer of a more complex blood vessel multi-stratum organization, which consists of smooth muscle cells, ECM and fibroblasts. Many mechanical and biological functions rely on this architecture that if recapitulated, would be crucial to the generation of a new class of *in vitro* engineered vascular structures. By encapsulating tissue specific cell populations in the outer hydrogel compartment, the proposed combination can be scaled to the generation of multicellular vascularized 3D organoids (such as hepatic lobules and bone osteons). This approach could also prospectively take advantage of spatially specific designs of hydrogel for each layer/compartment (e.g. localized biochemical signals or mechanical characteristic).

4. Conclusions

In this study a combination of SAM-based cell deposition and hydrogel photocrosslinking was proposed as a platform for engineering 3D tissue constructs, and specifically applied to the generation of hollow vascular structures. The cell deposition process was found to rely on two distinctive SAM desorption mechanisms: photoinduced and electrically triggered. The former, occurs concomitantly to hydrogel photocrosslinking with high efficiency eliminating the need for electrical connections and equipment. The latter better maintains cell morphology preserves monolayer features, and higher cell transfer efficiency over time.

In 3D, the combination of SAM-based cell transfer and hydrogel photocrosslinking enables a rapid single-step engineering of micrometric tubular constructs lined with an endothelial cell monolayer. The proposed approach can be used to design more challenging 3D vascular structures, such as double-layer constructs, representing therefore a potentially useful microengineering platform to mimic *in vivo* microvascular organization.

Acknowledgments

This research has been supported by the NIH (HL092836, AK; EB008392, AK; DE019024, AK; HL099073, AK; AR057837, YY; DE021468, YY), NSF and MEXT (Grant-in-Aid for Young Scientists (A), 20686056, Japan, JF). NS acknowledges support provided by the Fondazione Fratelli Agostino and Enrico Rocca through the Progetto Rocca Post Doctoral Fellowship. JF acknowledges support provided by JSPS through Excellent Young Researchers Overseas Visit Program.

References

1. Lovett M, Lee K, Edwards A, Kaplan DL. Vascularization strategies for tissue engineering. *Tissue Eng Part B Rev.* 2009; 15:353–70. [PubMed: 19496677]
2. Ko HC, Milthorpe BK, McFarland CD. Engineering thick tissues--the vascularisation problem. *Eur Cell Mater.* 2007; 14:1–18. discussion -9. [PubMed: 17654452]
3. McGuigan AP, Sefton MV. Vascularized organoid engineered by modular assembly enables blood perfusion. *Proc Natl Acad Sci U S A.* 2006; 103:11461–6. [PubMed: 16864785]
4. Wong KH, Truslow JG, Tien J. The role of cyclic AMP in normalizing the function of engineered human blood microvessels in microfluidic collagen gels. *Biomaterials.* 2010; 31:4706–14. [PubMed: 20303168]
5. Villalona GA, Udelsman B, Duncan DR, McGillicuddy E, Sawh-Martinez RF, Hibino N, et al. Cell-seeding techniques in vascular tissue engineering. *Tissue Eng Part B Rev.* 2010; 16:341–50. [PubMed: 20085439]
6. Norotte C, Marga FS, Niklason LE, Forgacs G. Scaffold-free vascular tissue engineering using bioprinting. *Biomaterials.* 2009; 30:5910–7. [PubMed: 19664819]
7. Seto Y, Inaba R, Okuyama T, Sassa F, Suzuki H, Fukuda J. Engineering of capillary-like structures in tissue constructs by electrochemical detachment of cells. *Biomaterials.* 2010; 31:2209–15. [PubMed: 20022631]
8. Fukuda J, Kameoka K, Suzuki H. Spatio-temporal detachment of single cells using microarrayed transparent electrodes. *Biomaterials.* 2011 in press.
9. Inaba R, Khademhosseini A, Suzuki H, Fukuda J. Electrochemical desorption of self-assembled monolayers for engineering cellular tissues. *Biomaterials.* 2009; 30:3573–9. [PubMed: 19362363]
10. Hannachi IE, Yamato M, Okano T. Cell sheet technology and cell patterning for biofabrication. *Biofabrication.* 2009; 1:022002. [PubMed: 20811100]
11. Khademhosseini A, Langer R, Borenstein J, Vacanti JP. Microscale technologies for tissue engineering and biology. *Proc Natl Acad Sci U S A.* 2006; 103:2480–7. [PubMed: 16477028]
12. Kachouie NN, Du Y, Bae H, Khabiry M, Ahari AF, Zamanian B, et al. Directed assembly of cell-laden hydrogels for engineering functional tissues. *Organogenesis.* 2010; 6:234–44. [PubMed: 21220962]
13. Ling Y, Rubin J, Deng Y, Huang C, Demirci U, Karp JM, et al. A cell-laden microfluidic hydrogel. *Lab Chip.* 2007; 7:756–62. [PubMed: 17538718]
14. Nichol JW, Koshy ST, Bae H, Hwang CM, Yamanlar S, Khademhosseini A. Cell-laden microengineered gelatin methacrylate hydrogels. *Biomaterials.* 2010; 31:5536–44. [PubMed: 20417964]
15. Van Den Bulcke AI, Bogdanov B, De Rooze N, Schacht EH, Cornelissen M, Berghmans H. Structural and rheological properties of methacrylamide modified gelatin hydrogels. *Biomacromolecules.* 2000; 1:31–8. [PubMed: 11709840]

16. Benton JA, DeForest CA, Vivekanandan V, Anseth KS. Photocrosslinking of gelatin macromers to synthesize porous hydrogels that promote valvular interstitial cell function. *Tissue Eng Part A*. 2009; 15:3221–30. [PubMed: 19374488]
17. Chen S, Cao Z, Jiang S. Ultra-low fouling peptide surfaces derived from natural amino acids. *Biomaterials*. 2009; 30:5892–6. [PubMed: 19631374]
18. Vacek K, Geimer J, Beckert D, Mehnert R. Radical generation from photoinitiator (IC 2959) decomposition and radical addition to acrylate. A laser photolysis Fourier transform electron paramagnetic resonance study. *J Chem Soc, Perkin Trans*. 1999; 2:2469–71.
19. Hennink WE, van Nostrum CF. Novel crosslinking methods to design hydrogels. *Adv Drug Deliv Rev*. 2002; 54:13–36. [PubMed: 11755704]
20. Nguyen KT, West JL. Photopolymerizable hydrogels for tissue engineering applications. *Biomaterials*. 2002; 23:4307–14. [PubMed: 12219820]
21. Huang J, Hemminger JC. Photooxidation of thiols in self-assembled monolayers on gold. *J Am Chem Soc*. 1993; 115:3342–3.
22. Love JC, Estroff LA, Kriebel JK, Nuzzo RG, Whitesides GM. Self-assembled monolayers of thiolates on metals as a form of nanotechnology. *Chem Rev*. 2005; 105:1103–69. [PubMed: 15826011]
23. Tarlov MJ, Burgess DRF, Gillen G. UV photopatterning of alkanethiolate monolayers self-assembled on gold and silver. *J Am Chem Soc*. 1993; 115:5305–6.
24. Brewer NJ, Janusz S, Critchley K, Evans SD, Leggett GJ. Photooxidation of Self-Assembled Monolayers by Exposure to Light of Wavelength 254 nm: A Static SIMS Study. *J Phys Chem B*. 2005; 109:11247–56. [PubMed: 16852373]
25. Brewer NJ, Rawsterne RE, Kothari S, Leggett GJ. Oxidation of Self-Assembled Monolayers by UV Light with a Wavelength of 254 nm. *J Am Chem Soc*. 2001; 123:4089–90. [PubMed: 11457164]
26. Norrod KL, Rowlen KL. Ozone-Induced Oxidation of Self-Assembled Decanethiol: Contributing Mechanism for “Photooxidation”? *J Am Chem Soc*. 1998; 120:2656–7.
27. Wildt B, Wirtz D, Searson PC. Programmed subcellular release for studying the dynamics of cell detachment. *Nat Methods*. 2009; 6:211–3. [PubMed: 19182793]
28. Okano T, Yamada N, Okuhara M, Sakai H, Sakurai Y. Mechanism of cell detachment from temperature-modulated, hydrophilic-hydrophobic polymer surfaces. *Biomaterials*. 1995; 16:297–303. [PubMed: 7772669]
29. Ernst O, Lieske A, Jager M, Lankenau A, Duschl C. Control of cell detachment in a microfluidic device using a thermo-responsive copolymer on a gold substrate. *Lab Chip*. 2007; 7:1322–9. [PubMed: 17896017]
30. Kumashiro Y, Yamato M, Okano T. Cell attachment-detachment control on temperature-responsive thin surfaces for novel tissue engineering. *Ann Biomed Eng*. 2010; 38:1977–88. [PubMed: 20387117]
31. Weder G, Guillaume-Gentil O, Matthey N, Montagne F, Heinzelmann H, Voros J, et al. The quantification of single cell adhesion on functionalized surfaces for cell sheet engineering. *Biomaterials*. 2010; 31:6436–43. [PubMed: 20621765]
32. Goldstein AS, DiMilla PA. Examination of membrane rupture as a mechanism for mammalian cell detachment from fibronectin-coated biomaterials. *J Biomed Mater Res A*. 2003; 67:658–66. [PubMed: 14566810]
33. Huang H, Dong CY, Kwon HS, Sutin JD, Kamm RD, So PT. Three-dimensional cellular deformation analysis with a two-photon magnetic manipulator workstation. *Biophys J*. 2002; 82:2211–23. [PubMed: 11916876]
34. Yang S, Saif T. Micromachined force sensors for the study of cell mechanics. *Rev Sci Instrum*. 2005; 76:044301–8.
35. Reinhart-King CA, Dembo M, Hammer DA. The dynamics and mechanics of endothelial cell spreading. *Biophys J*. 2005; 89:676–89. [PubMed: 15849250]
36. Ryan PL, Foty RA, Kohn J, Steinberg MS. Tissue spreading on implantable substrates is a competitive outcome of cell-cell vs. cell-substratum adhesivity. *Proc Natl Acad Sci U S A*. 2001; 98:4323–7. [PubMed: 11274361]

37. Okochi N, Okazaki T, Hattori H. Encouraging effect of cadherin-mediated cell-cell junctions on transfer printing of micropatterned vascular endothelial cells. *Langmuir*. 2009; 25:6947–53. [PubMed: 19453131]
38. Flynn NT, Tran TNT, Cima MJ, Langer R. Long-Term Stability of Self-Assembled Monolayers in Biological Media. *Langmuir*. 2003; 19:10909–15.
39. Dejana E, Tournier-Lasserre E, Weinstein BM. The control of vascular integrity by endothelial cell junctions: molecular basis and pathological implications. *Dev Cell*. 2009; 16:209–21. [PubMed: 19217423]
40. Johnstone S, Isakson B, Locke D. Biological and biophysical properties of vascular connexin channels. *Int Rev Cell Mol Biol*. 2009; 278:69–118. [PubMed: 19815177]
41. Provost N, Moreau M, Leturque A, Nizard C. Ultraviolet A radiation transiently disrupts gap junctional communication in human keratinocytes. *Am J Physiol Cell Physiol*. 2003; 284:C51–9. [PubMed: 12388105]
42. Laird DW. Connexin phosphorylation as a regulatory event linked to gap junction internalization and degradation. *Biochim Biophys Acta*. 2005; 1711:172–82. [PubMed: 15955302]
43. Kawashima T, Yokoi T, Kaji H, Nishizawa M. Transfer of two-dimensional patterns of human umbilical vein endothelial cells into fibrin gels to facilitate vessel formation. *Chem Commun (Camb)*. 2010; 46:2070–2. [PubMed: 20221495]
44. Kobayashi A, Miyake H, Hattori H, Kuwana R, Hiruma Y, Nakahama K, et al. In vitro formation of capillary networks using optical lithographic techniques. *Biochem Biophys Res Commun*. 2007; 358:692–7. [PubMed: 17509527]
45. Chrobak KM, Potter DR, Tien J. Formation of perfused, functional microvascular tubes in vitro. *Microvasc Res*. 2006; 71:185–96. [PubMed: 16600313]
46. Price GM, Wong KH, Truslow JG, Leung AD, Acharya C, Tien J. Effect of mechanical factors on the function of engineered human blood microvessels in microfluidic collagen gels. *Biomaterials*. 2010; 31:6182–9. [PubMed: 20537705]
47. Chiu JJ, Chien S. Effects of disturbed flow on vascular endothelium: pathophysiological basis and clinical perspectives. *Physiol Rev*. 2011; 91:327–87. [PubMed: 21248169]

Appendix

Figures with essential color discrimination. Figure 1, 3, 5 and 6 in this article have parts that are difficult to interpret in black and white. The full color images can be found in the on-line version, at

- We combined SAM-based cell transfer and hydrogel photopatterning techniques.
- We identified two SAM desorption mechanisms: photoinduced and electrically triggered.
- Cell transfer was efficient and preserved cell viability and monolayer features.
- Vascular-like constructs lined with an endothelial cell monolayer were generated.
- Double-layered constructs were photopatterned for mimicking arterioles organization.

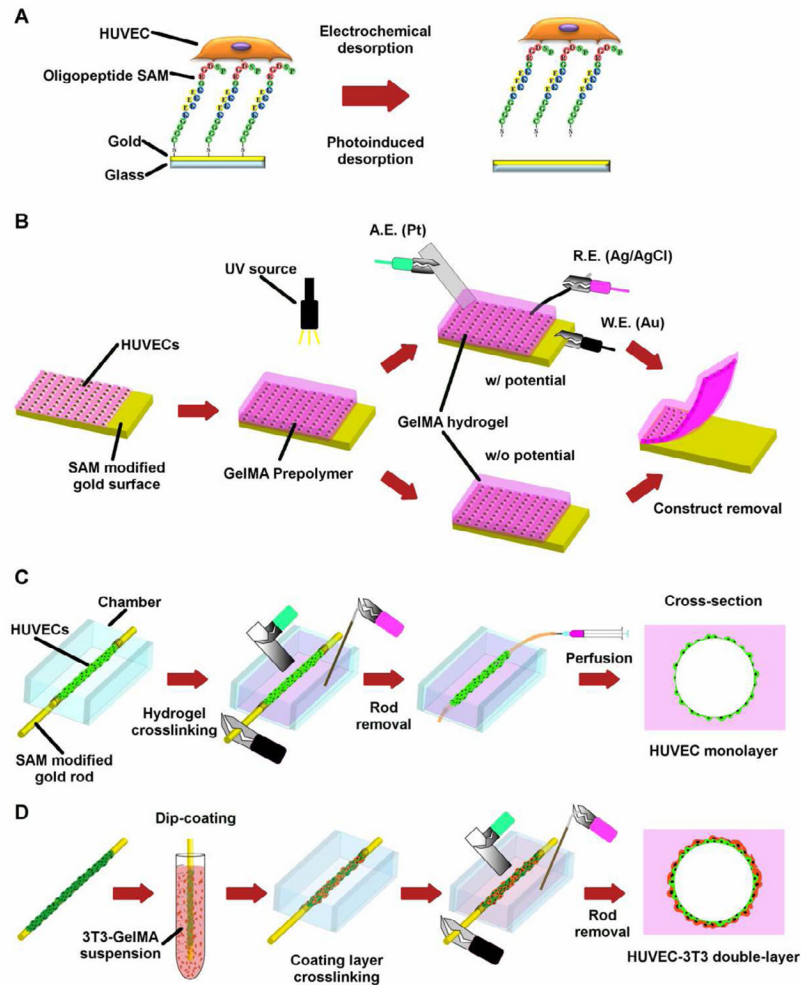


Fig. 1. Cell transfer and vascular construct generation schematic. (A) The oligopeptide CGGGKEKEKEKGRGDSP was chemically adsorbed onto a gold surface and seeded with HUVECs. SAM desorption from the surface resulted in cell detachment. (B) HUVECs seeded on gold substrates modified with oligopeptide based-SAM were transferred to the hydrogel after GelMA prepolymer photocrosslinking with or without electrical potential. (C) Micrometric gold rods enveloped with cells were positioned in culture chambers that were then filled with GelMA. After photocrosslinking, an electrical potential was applied and the endothelial cells were transferred. Following rod removal, the device was connected to a microsyringe pump and cultured under perfusion. (D) Double-layer cell microvascular structures were generated by dip-coating the gold rods enveloped with HUVECs in a GelMA solution containing 3T3 cells. The double-layered rods were then encapsulated in the hydrogel, cells were transferred by electrical potential application to the gel and the rod was removed.

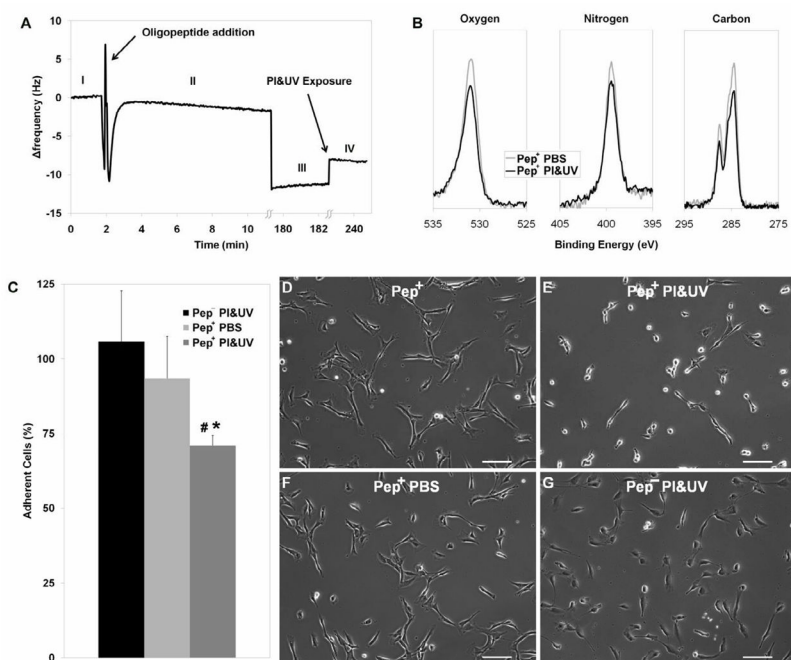


Fig. 2. Effect of PI&UV on SAM and HUVEC adhesion. (A) Resonant frequency of bare gold surface (I) decreased with oligopeptide adsorption over time (II, 10 min; III, 180 min), and increased after PI&UV exposure, due to mass desorption (IV). (B) XPS surface analyses show decreased Oxygen, Nitrogen and Carbon peaks after PI&UV exposure. (C) Percentage of adherent HUVECs on modified substrates upon exposure to PI&UV (Pep⁺ PI&UV) show almost 30% cell detachment as compared to non-modified substrates (Pep⁻ PI&UV) or modified substrates exposed to PBS (Pep⁺ PBS). Representative phase contrast images show that HUVECs adhering on modified substrates (D) acquire a rounded morphology after PI&UV (E). The cells maintained a spread morphology on modified substrates when exposed to PBS (F) or on non-modified substrates when exposed to PI&UV (G). PI&UV exposure induce loss of fraction of the adsorbed SAM leading to partial cell detachment. (Error bars: \pm SD; statistically significant difference from Pep⁺ PBS # and Pep⁻ PI&UV *)

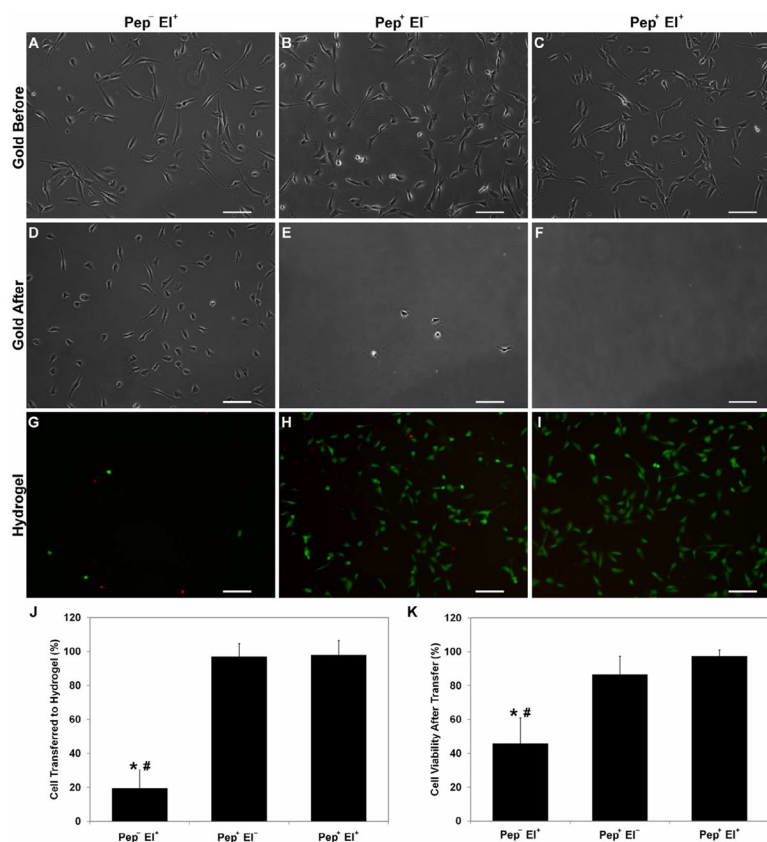


Fig. 3. Cell transfer from gold substrate to hydrogel. Cells were transferred from non-modified substrates with electrical potential ($\text{Pep}^- \text{EI}^+$), modified substrates without electrical potential ($\text{Pep}^+ \text{EI}^-$), and modified substrate with electrical potential ($\text{Pep}^+ \text{EI}^+$). Representative phase contrast images of the same substrate before (A–C) and after (D–E) transfer show negligible number of cells still adherent on peptide coated gold after transfer as opposed to the high number of cells on non-modified substrates. The corresponding fluorescent images (GFP/EthD-1) of the hydrogels after transfer display few rounded cells for the $\text{Pep}^- \text{EI}^+$ (G) and numerous viable spread HUVECs for both $\text{Pep}^+ \text{EI}^-$ (H) and $\text{Pep}^+ \text{EI}^+$ (I). (J) Mean percentage of cell transferred to hydrogel confirms that peptide modification enables complete HUVEC transfer as compared to only 20% of cells for $\text{Pep}^- \text{EI}^+$. (K) Mean cell viability after transfer similarly illustrates that both modified substrates promoted transfer with high cell viability as opposed to non-modified ones (less than 50% viable cells). Gold surface coating with oligopeptide SAM enables HUVEC transfer to GelMA hydrogels with high efficiency and viability independent of electrochemical SAM desorption. (Scale bars: 100 μm ; error bars: \pm SD; statistically significant difference from $\text{Pep}^+ \text{EI}^-$ # and $\text{Pep}^+ \text{EI}^+$ *)

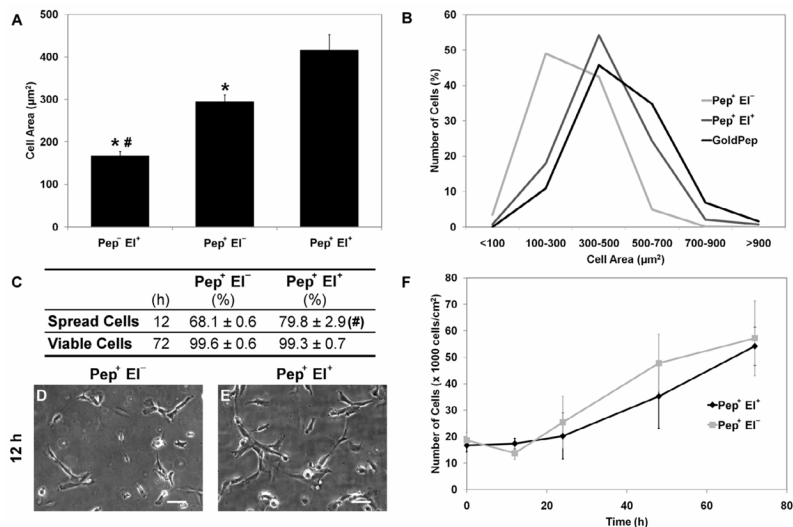


Fig. 4. Cell morphology and proliferation upon transfer. (A) Mean cell area after transfer shows that Pep⁻ EI⁺ cells occupy significantly smaller area than Pep⁺ EI⁻ and Pep⁺ EI⁺, the latter being statistically more spread among the modified substrates. (B) Cell area distribution shows that cells transferred from the modified substrates using potential (Pep⁺ EI⁺) maintained a similar morphology whereas those transferred without potential (Pep⁺ EI⁻) tended to be less spread than on gold substrates. (C) Similarly, a higher percentage (Mean \pm SD) of cells (E) presented a spread morphology at 12 h on Pep⁺ EI⁺ hydrogels compared to cells on Pep⁺ EI⁻ (D). However, electrochemical oligopeptide cleavage did not show significant effect on the percentage (Mean \pm SD) of viable cells (C) and on proliferation (F) after transfer. While electrochemical SAM desorption has an effect on the cell morphology immediately after transfer, no differences are evidenced on longer cultures both conditions maintaining proliferative cell population. (Scale bars: 50 μm ; error bars: \pm SD; statistically significant difference from Pep⁺ EI⁻ # and Pep⁺ EI⁺ *)

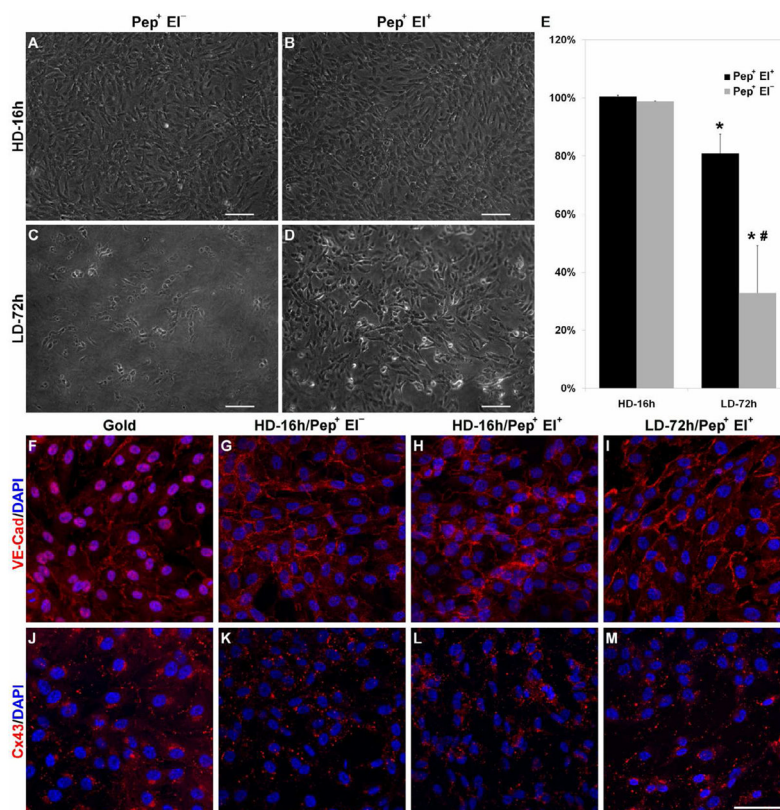


Fig. 5. HUVEC monolayer transfer. Representative phase contrast images of hydrogels after transfer from modified substrates seeded at high density and cultured for 16 h (HD-16h) (A,B) or at low density and cultured for 72 h (LD-72h) (C,D) transferred either without (A,C) or with (B,D) potential. (E) Mean percentage of cells transferred to hydrogel decreases upon longer culture, maintaining however high transfer efficiency (over 80%) when SAM was electrochemically desorbed ($\text{Pep}^+ \text{EI}^+$). (F–M) Representative confocal images of gold and hydrogel samples show intact VE-Cad junctions while Cx43 is mostly internalized upon transfer. Both processes were not affected by transfer method and culture period on gold. Although endothelial monolayers can be transferred both with and without electrical potential, the longer culture requires electrochemical oligopeptide cleavage for efficient transfer. (Scale bars: 100 μm ; error bars: \pm SD; statistically significant difference between culture period * and between transfer protocol #)

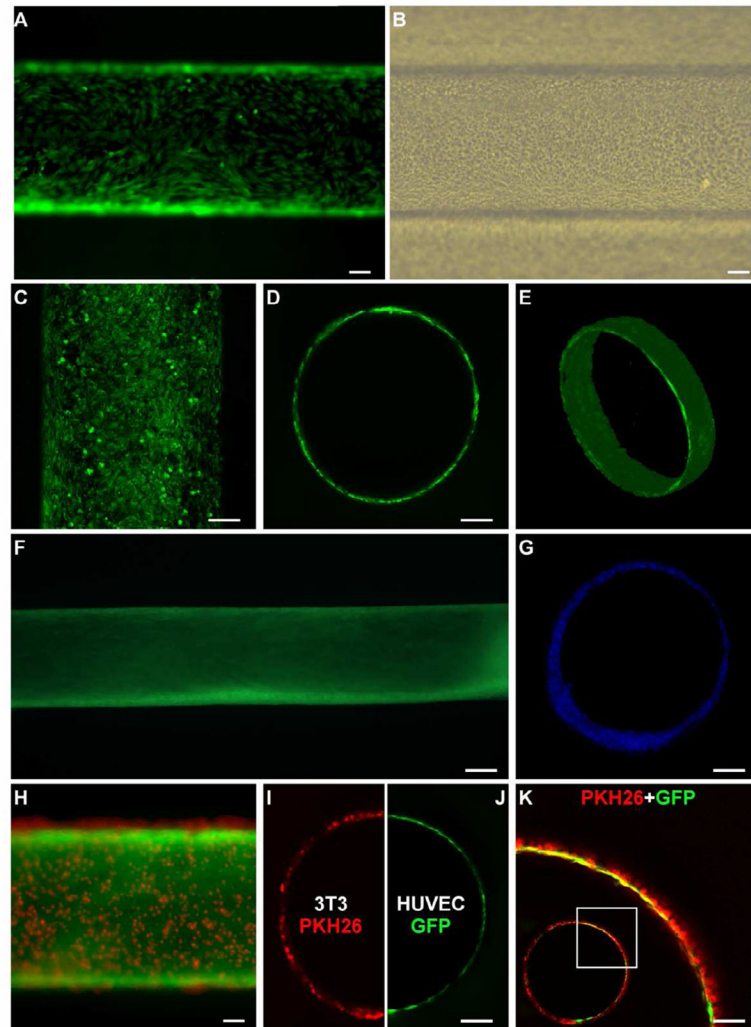


Fig. 6. Fabrication of microvascular-like structures. (A) HUVECs were cultured on gold rods for three days to create a confluent monolayer. (B) After GelMA photocrosslinking, electrical potential application and rod removal, HUVECs were transferred uniformly on the hydrogel channel surface. (C) The constructs, cultured under perfusion, maintained a continuous endothelial monolayer lining the surface of the channel (D) mimicking the 3D endothelial cell organization in microvasculature (E). (F) Over 5 days of culture, the constructs maintained a stable shape and a compact cell layer on the channel surface. (G) After 15 days of culture, samples stained with DAPI and cross-sectioned displayed a hollow channel structure that was maintained over long term culture. (H) GelMA encapsulated PKH26-stained 3T3 cells photopatterned on HUVEC monolayer seeded on gold rods. (I) Confocal image showing cross-section of hydrogel channel covered with 3T3 cells, (J) lined with HUVEC monolayer. (K) Magnified merged confocal image shows both 3T3 (PKH26) and HUVEC (GFP) layer patterned in close proximity (inset shows the entire channel). (All scale bars: 100 μm , except F: 200 μm).